"BABEŞ-BOLYAI" UNIVERSITY OF CLUJ-NAPOCA, ROMANIA
FACULTY OF CHEMISTRY AND CHEMICAL ENGINEERING

ALLOYS WITH IMPROVED CORROSION RESISTANCE OBTAINED, OR TREATED BY ELECTROCHEMICAL WAY

PhD Thesis Abstract

PhD student:

Diana BLEJAN

Scientific advisor:

Prof. Dr. Liana-Maria MUREŞAN

CLUJ-NAPOCA

2012

Investing in people!
Ph.D. scholarship, Project co-financed by the SECTORAL OPERATIONAL PROGRAM FOR HUMAN RESOURCES DEVELOPMENT 2007 - 2013
Priority Axis 1. "Education and training in support for growth and development of a knowledge based society"
Key area of intervention 1.5: Doctoral and post-doctoral programs in support of research.
Contract nr.: **POSDRU/88/1.5/S/60185 –** "INNOVATIVE DOCTORAL STUDIES IN A KNOWLEDGE BASED SOCIETY"
Babeş-Bolyai University, Cluj-Napoca, Romania

"BABEŞ-BOLYAI" UNIVERSITY OF CLUJ-NAPOCA FACULTY OF CHEMISTRY AND CHEMICAL ENGINEERING
DEPARTMENT OF PHYSICAL CHEMISTRY

DIANA BLEJAN

ALLOYS WITH IMPROVED CORROSION RESISTANCE OBTAINED, OR TREATED BY ELECTROCHEMICAL WAY

PhD Thesis Abstract

Jury

President:

Prod. Conf. Dr. Cornelia MAJDIK, Babeş-Bolyai University, Cluj-Napoca.

Scientific advisor:

Prof. Dr. Liana-Maria MUREŞAN

Members:

Prof. Dr. Ingrid MILOŠEV, Jožef Stefan Institute, Ljubljana, Slovenia

Prof. Dr. Nicolae VASZILCSIN, University Politehnica, Timisoara

Prof. Dr. Ionel Cătălin POPESCU, Babeş-Bolyai University, Cluj-Napoca

Defense:.25th of September 2012

TABLE OF CONTENTS

INTRODUCTION

Alloys are materials obtained by combining two or more metals or non-metals in order to improve their properties. The physical properties, such as density, reactivity, Young's modulus, and electrical and thermal conductivity of an alloy may not differ greatly from those of its elements, but engineering properties such as tensile strength, shear strength, or corrosion resistance may be substantially different from those of the constituent materials.

One of the ways to improve the corrosion resistance of zinc coatings consists in alloying zinc with group eight metals (Fe, Co, Ni) [1-5]. Thus, Zn-Ni alloys provide superior sacrificial protection to steel than pure zinc since they corrode more slowly, and are successfully used especially in the automobile and aeronautical industry [6] as a substitute for toxic and high-cost cadmium coatings [7].

An alternate way for further enhancing the corrosion resistance of zinc coatings on steel consists in generating composite coatings on its surface by electrolysis of plating solutions, in which micron or sub-micron size particles (*i.e.* TiO_2, SiO_2, Al_2O_3 etc.) are suspended [3, 8].

On the other hand, titanium alloys are today one of the most important metallic materials used in orthopedics and dental surgery given their good biocompatibility and corrosion resistance [9, 10].

In this context, the aim of this work was on one side:

(i) to obtain and to investigate composite layers of Zn-Ni alloy with TiO_2 and Al_2O_3 nanoparticles prepared on steel, by using co-electrodeposition method

and one the other hand,

(ii) to prepare TiO_2 films on Ti and Ti alloys by anodization method, in order to improve their anticorrosive properties.

The personal contributions described in this thesis are divided in two parts. The first part has been focused on obtaining and characterization of nanocomposite Zn-Ni coatings; the second part deals with deposition of TiO_2 layer on Ti and its alloys.

The original results are presented into three sections as follows:

i) *Zn-Ni composite coatings on steel electrodeposited from an alkaline home-made electrolyte.* This part presents the results concerning the use of different combinations of additives and the influence of TiO_2 nanoparticles on the anticorrosive properties of Zn-Ni layers prepared from an original electrolyte.

ii) Zn-Ni-nanoparticles composite coatings on steel electrodeposited from a commercial alkaline electrolyte. The section is focused on improving of corrosion resistance of Zn-Ni coating by embedding TiO_2 and Al_2O_3 nanoparticles.

iii) Ti and Ti alloys treated by anodic oxidation in 1M acetic acid. The third part, presents the effect on corrosion behavior of potentiostatic anodization in acetic acid of three titanium-based materials (titanium metal, and Ti−6Al−7Nb and Nitinol alloys) in simulated physiological solution.

The corrosion behavior of the alloys was investigated by electrochemical and non-electrochemical methods.

Keywords: Zn-Ni alloy, Zn-Ni-nanoparticles composite, electrodeposition, Ti and Ti alloys, anodization, corrosion

PART II.

ORIGINAL CONTRIBUTIONS

4. Zn-Ni composite coatings on steel electrodeposited from an alkaline home-made electrolyte

In this study was investigated the influence of several additives such as polyethylene glicol (PEG), coumarin, piperonal, and vanillin on the quality of Zn-Ni deposits obtained by electrodeposition from an alkaline bath containing triethanolamine. The most efficient additives (PEG and vanilline) were used further in order to obtain composite Zn-Ni-TiO_2 coatings, by co-deposition of the two metals with TiO_2 nanoparticles.

4.1. Experimental conditions

The Zn-Ni alloys have been electrodeposited form an alkaline home-made electrolyte (pH 13) containing 15 g/L ZnO (Merck, Germany), 130 g/L NaOH (Merck, Germany), 80 g/L triethanolamine (TEA) (Sigma-Aldrich, Germany) and 6 g/L $Ni_2SO_4 \cdot 6H_2O$ (Reactivul Bucuresti). Polyethylene glycol, coumarin, piperonal, and vanillin (Sigma-Aldrich, Germany) have been tested as brightening agents. TiO_2 nanoparticles (Degussa, 99.5%, 21 nm,) were added into the plating bath in different concentrations in order to obtain composite Zn-Ni-TiO_2 coatings.

The electrodeposition of Zn-Ni coatings was carried out at i = 20 and 40 mA/cm^2, during 30 and 35 minutes, under mechanical stirring (200 rpm) in a two compartment glass cell, using a steel (OL37) disc electrode as working electrode, (S = 0.5024 and 0.785 cm^2), a $Ag/AgCl/KCl_{sat}$ as reference electrode and a Pt foil as a counter electrode. Before using, the working electrode was wet ground on emery paper of different granulation and finally polished with a suspension of alumina. The electrode was ultrasonicated for 2 minutes, washed with acetone and distilled water in order to remove the impurities from the surface.

For evaluation of corrosion resistance, open circuit potential measurements and polarization curves recorded at a scan rate of 0.166 mV/s were carried out in 0.2 g/L Na_2SO_4 pH = 5.

The deposit structure and the preferred orientation of crystallites were determined by X-ray diffraction (XRD) analysis and the deposit morphology was determined with a scanning

electron microscope (SEM) (Philips XL-30). The chemical composition of the nanocomposite films was determined by using an EDAX NEW XL30 (Philips) X-ray dispersive energy analyzer attached to the SEM.

4.2. Influence of additives on Zn-Ni electrodeposition

It was concluded that all additives improved the quality of Zn-Ni deposits in terms of adherence, grain size and homogeneity. The most leveled and brightest deposits were obtained in the presence of a combination of PEG (3 ml/L) and vanillin and, as expected, the brightness increased with the concentration of vanillin [11].

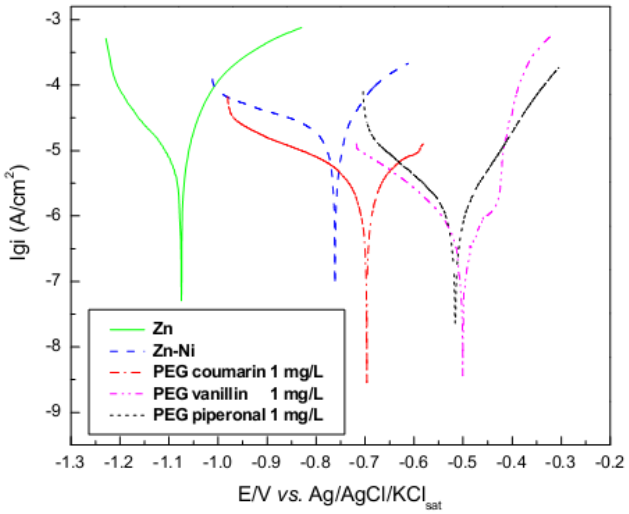

Figure 4.4. Polarization curves for Zn-Ni coated steel obtained from a bath containing different additives. *Experimental conditions:* electrolyte 0.2 g/L Na_2SO_4 (pH 5); scan rate, 0.166 mV/s.

The addition of additives shows a significant decrease of corrosion current densities compared to Zn and Zn-Ni obtained without additives. The values of the corrosion parameters of the coatings prepared in the absence and in the presence of additives were calculated from the polarization curves by using the Stern - Geary theory [12] and Tafel interpretation and are presented in Table 4.1. One can notice that the additives shift the corrosion potential towards more positive values and decrease the current with about one order of magnitude. When used in concentration of 1 mg/L in combination with PEG, coumarin and vanillin led to similar results in terms of corrosion rate, but the deposits obtained in the presence of vanillin were brighter and had a higher polarization resistance than those obtained in the presence of coumarin [11].

Table 4.1. Parameters of the corrosion process of the Zn and Zn-Ni coatings

Parameters	Zn	Zn-Ni	Zn-Ni + PEG +coumarin	Zn-Ni + PEG + piperonal		Zn-Ni + PEG + vanillin		
			1mg/L	1mg/L	5mg/L	1mg/L	5mg/L	10mg/L
i_{corr} (A/cm^2)	$5.80*10^{-6}$	$1.68*10^{-6}$	$3.44*10^{-7}$	$1.68*10^{-6}$	$1.00*10^{-6}$	$3.34*10^{-7}$	$4.95*10^{7}$	$4.07*10^{-7}$
b_c (V/dec)	0.034	0.074	0.040	0.085	0.118	0.056	0.034	0.053
b_a (V/dec)	0.084	0.047	0.050	0.112	0.048	0.046	0.038	0.005
Rp ($\Omega.cm^2$)	438	441	911	618	9976	6948	3315	4865
E_{corr} (V)	- 1.075	- 0.761	- 0.622	- 0.516	- 0.530	- 0.501	- 0.541	- 0.438
V_{corr} (mm/an)	$1.16*10^{-1}$	$2.51*10^{-2}$	$5.13*10^{-3}$	$2.51*10^{-2}$	$1.49*10^{-2}$	$4.98*10^{-3}$	$7.38*10^{-3}$	$6.05*10^{-3}$

4.3.2. Electrodeposition of Zn-Ni-TiO_2 coatings

To obtain more corrosion resistant Zn-Ni coatings, composite coatings were prepared by introducing various concentrations (3, 5 and 10 g/L) of TiO_2 nanoparticles in the plating baths [13].

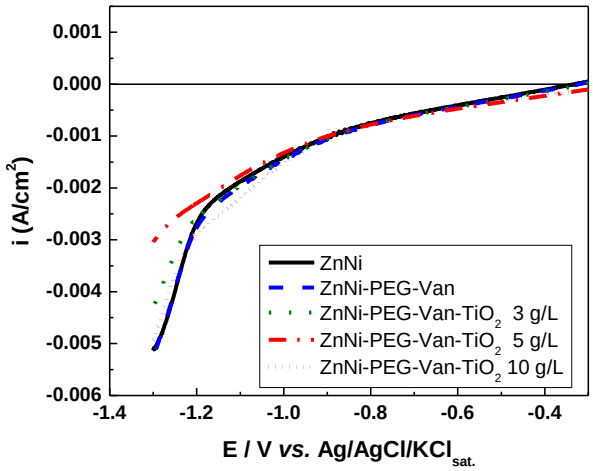

Figure 4.11. Polarization curves obtained during Zn-Ni electrodeposition in the absence and in the presence of TiO_2 nanoparticles. Scan rate, 50 mV/s.

As seen from polarization curves recorded during the electrodeposition of Zn-Ni coatings (Figure 4.11), no significant changes are observed in the kinetically controlled region of the curves when adding TiO_2 nanoparticles or when modifying the concentration, while a slight increase of the current density is noticed in the mixed-control region. This could be due to a catalytic phenomenon initiated by defects and dislocations or to chemical heterogeneities generated in the metallic matrix by the embedded particles at high overpotentials.

4.3.3.2. X-ray diffraction

In order to put on evidence the formation of Zn-Ni alloy by electrodeposition and to correlate the electrochemical results with the structural data of the coatings, XRD investigations were carried out on the coated steel electrodes obtained with PEG and 1 mg/L of different additives (Figure 4.14).

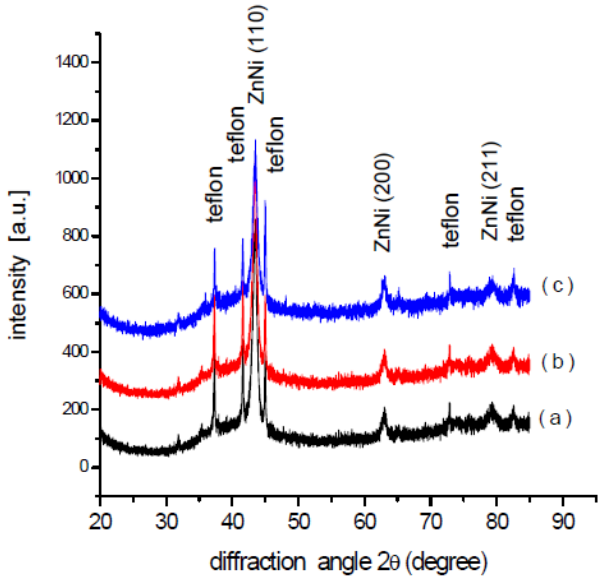

Figure 4.14. X-ray diffractograms of Zn-Ni coatings obtained from a bath containing PEG (3 ml/L) in combination with piperonal (a), vanillin (b) and cumarin (c) in concentration 1 mg/L.

In Table 4.7 are presented the microstructural parameters, the effective crystallite mean siye, D_{eff} (nm) and the mean root square (rms) of the microstrains , $\langle \varepsilon^2 \rangle_m^{1/2}$, of the Zn-Ni cubic crystalline phase of the Zn-Ni coatings.

Table 4.7. Microstructural parameters of the Zn-Ni coatings obtained from a bath containing with PEG (3 ml/L) in combination with piperonal (a), vanillin (b) and coumarin (c) in concentration 1 mg/L.

Sample	Unit cell parameter a [nm]	Unit cell volume [nm^3]	Effective crystallite mean size D_{eff} (nm)	Rms of the microstrains $\langle \varepsilon^2 \rangle_m^{1/2}$ x 10^3
Zn-Ni + PEG + piperonal	0.2958(2)	0.2588(7)	**8.85**	**5.093**
Zn-Ni + PEG + vanillin	0.2955(6)	0.2581(9)	**8.45**	**4.574**
Zn-Ni + PEG +coumarin	0.2957(7)	0.2587(4)	**9.62**	**2.424**

The nanostructured Zn-Ni coatings prepared in the presence of additives piperonal and vanillin showed a smaller average size of the crystallites (8.4-8.8 nm), than the nanostructured Zn-Ni coatings prepared in the presence of coumarin (9.6 nm). At the same time, the lattice microstrain $< \varepsilon^2 >^{1/2}$ of nanostructured Zn-Ni coatings prepared in the presence of piperonal and vanillin shows a larger value of the intercrystallite zones that suggests a higher interaction between the nanoparticles of the coating and the steel support and, consequently, a higher corrosion resistance of the coatings.

Morfo-structural study of the Zn-Ni coatings

For we see wich is the nanoparticles influence on structure and morphology of the Zn-Ni deposited further, are presented the diffraction spectres obtained of some deposits where the additives were PEG and Van [13].

The examined samples were as follows:

ZnNi (S_{01})

ZnNi + 3 ml/L PEG + 10 mg/L Van (S_0)

ZnNi + 3 ml/L PEG + 10 mg/L Van + 5 g/L TiO_2 (S_5)

ZnNi + 3 ml/L PEG + 10 mg/L Van + 10 g/L TiO_2 (S_{10})

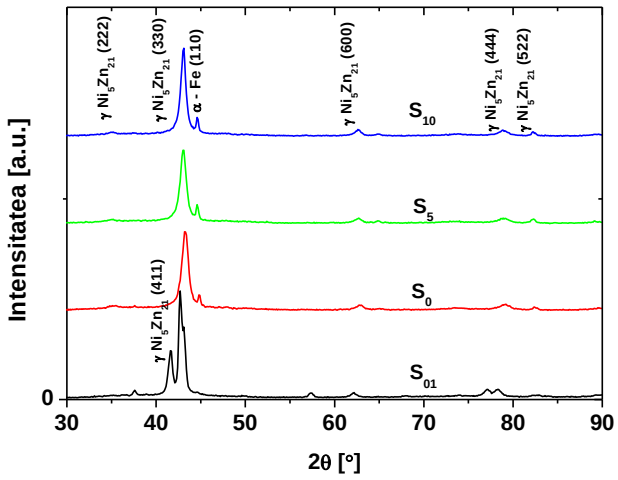

Figure 4.15. XRD of samples S_{01} (in the absence of brightening agents and of TiO_2), S_0 (in the absence of TiO_2 nanoparticles, x=0), S_5 and S_{10} (for 5 g/L and respectively 10 g/L TiO_2 nanoparticles).

As we can see from Figure 4.15, the diffraction peaks for all samples obtained by using brightening agents and TiO_2 nanoparticles correspond only to γ-phase (Ni_5Zn_{21}). It is well-known that the high corrosion resistance of the Zn–Ni coatings might primarily be attributed to the existence of this phase. The absence of TiO_2 peaks in the XRD spectra suggests that the concentration of phases associated with the nanoparticles is under the limit of detection of XRD method. The obtained results are in accordance with those reported for alloys containing 19–20 at. % Ni [3] and with the zinc–nickel phase diagram for γ-Ni_5Zn_{21}[8].

Another aspect that should be emphasized is related to the crystal orientation in the deposit, which is considered to be an important factor in the corrosion process. It is common knowledge that the intensity of XRD peaks (characterized by Miller indices (hkl)) is proportional to the density of oriented lattice planes. Consequently, the change of the grain orientations in presence of nanoparticles is indicated by changes of peak intensities. In the same time, the metal local coordination is correlated with planar packing densities.

In the case of investigated Zn-Ni coatings, the small change in the intensities ratio I(330)/(I(330)+I(600)), presented in Table 4.8., shows the absence of textural modifications of deposits in the presence of TiO_2 nanoparticles.

The high value of the intensities ratio I(330)/(I(330)+I(600)) suggests a good packing. Valoarea mare a raportului intensităţilor $I_{(330)}/(I_{(330)}+I_{(600)})$, sugerează o densitate bună de împachetare associated to more closely packed (330)) (or (110)) planes. The XRD pattern of sample S_{10} is similar with the result reported for pure γ-phase deposits obtained from alkaline solutions [14].

Table 4.8. Parameters obtained from XRD measurements.

Sample	$\frac{I(330)}{I(330)+I(600)}$ %	D [nm]
S_{01}	92	14.0
S_0 (0 g/L TiO_2)	94	11.4
S_5 (5 g/L TiO_2)	95.5	10.7
S_{10} (10 g/L TiO_2)	95	11.9

The calculated value for D (see Table 4.8.) shows that the grain size decreases with increasing concentration of TiO_2 nanoparticles up to 5 g/L TiO_2, and slightly increases for 10 g/L. The decrease of grain dimensions is due to the fact that the nanoparticles influence the competitive formation of metal nuclei and crystal growth. The TiO_2 nanoparticles disturb the regular growth of metallic crystals and causes new nucleation sites to appear.

4.3.4. Electrochemical corrosion of composite Zn-Ni-TiO_2 layer obtained by electrodeposition

Irrespective of the deposition mechanism, the Ni and TiO_2 presence and concentration in the deposit strongly influences the corrosion behavior of the alloy.

4.3.4.1. Open circuit potential

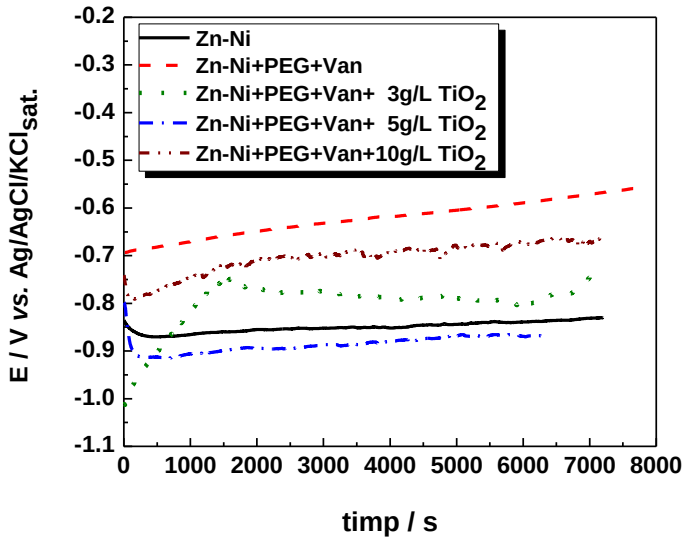

Figure 4.18. Evolution of open circuit potentials for Zn-Ni coatings obtained in the absence and in the presence of TiO_2 nanoparticles, after immersion in 0.2 g/L Na_2SO_4 (pH 5).

As expected, as we can see in Figure 4.18, the OCP values noticed for Zn-Ni alloy are more positive than those observed in the same conditions for pure Zn coatings [14], suggesting a more noble character of the deposit, which could be associated to an inhibition of the anodic reaction and consequently to a higher corrosion resistance. The most positive value was recorded in the case were used only PEG and Van.

A shift of the OCP values towards more positive potentials is observed in some cases when TiO_2 nanoparticles were present in the plating bath, as compared to Zn-Ni coatings obtained without additives, suggesting an interaction of TiO_2 with the anodic reaction of the corrosion process [13].

4.3.4.2. Polarization curves (PC)

Linear polarization measurements performed in a potential range of ± 20 mV *vs. ocp* allowed the evaluation of the polarization resistance, R_p (Table 4.9).

The higher values noticed in the presence of TiO_2 are probably due to lowering of the surface area of the electrode by embedded particles [6], and to structural changes induced by them. However, it should be mentioned that an increase of TiO_2 concentration beyond 3 g/L does not lead to further increase of R_p, probably due to defects and dislocations generated by the inclusion of nanoparticles in the metallic matrix.

Table 4.9. Polarization resistance values for Zn-Ni-TiO_2 deposited.

Sample	Electroplating solution	R_p ($\Omega.cm^2$)
S_{01}	Zn-Ni	8138
S_0	Zn-Ni+PEG+Van	8305
S_{03}	Zn-Ni+PEG+Van - 3 g/L TiO_2	9995
S_{05}	Zn-Ni+PEG+Van - 5 g/L TiO_2	9411
S_{10}	Zn-Ni+PEG+Van - 10 g/L TiO_2	9033

The results of the polarization tests are presented in Table 4.10. The tests were carried out in a potential range of ± 200 mV *vs.* OCP.

Table 4.10. Kinetics parameters of the corrosion process of Zn-Ni alloy obtained from baths containing additives and TiO_2 nanoparticles at different concentrations.

Electrode	Zn-Ni	ZnNi+PEG + Van	ZnNi+PEG+ Van+ 3 g/L TiO_2	ZnNi+PEG+ Van+ 5 g/L TiO_2	ZnNi+PEG+ Van+ 10 g/L TiO_2
i_{corr} (A/cm^2)	$4.0 * 10^{-5}$	$6.3 * 10^{-5}$	$5.0 * 10^{-5}$	$2.0 * 10^{-5}$	$1.0 * 10^{-5}$
b_a (V/dec)	25.13	11.86	2.00	17.07	13.37
b_c (V/dec)	2.30	2.18	10.46	4.26	13.18
E_{corr} (V/SCE)	- 0.848	- 0.469	- 0.717	- 0.646	- 0.601

As noticed, the addition of PEG and Vanillin in the plating bath gives rise to significant decrease of corrosion current density as compared to Zn-Ni obtained without additives. This indicates that, as expected, the organic compounds strongly modified the quality of the cathodic deposit in terms of structure and morphology, producing more compact, fine-grained and consequently more corrosion resistant coatings. In terms of the effect of TiO_2 nanoparticles, the addition of inert nanoparticles led to a decrease of corrosion current densities only in comparison with the pure Zn-Ni coating obtained from solution without additives. The decrease of corrosion currents could be due either to grain refinement of the deposit (see D values in Table 4.8), or to the fact that the incorporation of inert TiO_2 nanoparticles in the coatings isolates them from the corrosion medium and distracts the corrosion current.

Due to the fact that the results obtained with the home-made electrolyte in the presence of TiO_2 nanoparticles were not satisfactory, further to study the possibility of obtained Zn-Ni composite coatings with and without TiO_2 and Al_2O_3 nanoparticles by using a commercial electrolyte (PERFORMA 280.5, COVENTYA S.A.S, France).

5. Zn-Ni-nanoparticles composite coatings on steel electrodeposited from a commercial alkaline electrolyte

5.1. Experimental conditions

Zn-Ni alloy was deposited from a commercial alkaline electrolyte (PERFORMA 280.5, COVENTYA S.A.S, France,) containing 82.6 g/L NaOH, 106 g/L ZINCATE 75 (containing 75 g/L Zn and 400 g/L NaOH), 12 mL PERFORMA 285 Ni-CPL, 100 mL PERFORMA 285 BASE, 2 mL PERFORMA Universal and 0.7 mL PERFORMA Addtive K (pH 13). After preparation, the electrolyte was analyzed by atomic absorbtion spectroscopy, finding a Zn content 0.795 g/L and Ni content of 1.392 g/L. TiO_2 nanoparticles were added into the plating bath in order to obtain composite Zn-Ni coatings. The concentration of TiO_2 nanoparticles were 0 (sample S_0), 3 g/L (sample S_3), 5 g/L (sample S_5) and 10 g/L (Sample S_{10}), respectively.

Experimental conditions were the follows: i = 20 mA/cm^2, deposition time 30 min, S = 0.5024 cm^2, stirring 200 rpm, at temperature 22 ± 1ºC.

The corrosion resistance of the deposits was evaluated comparatively by electrochemical measurements: open circuit potential (recorded for 1 hour, until it was stabilized), polarization curves.

The deposit morphology was determined with scanning electron microscope (SEM). The chemical composition of the nanocomposite films was determined by using an EDAX NEW XL30 (Philips) X-ray dispersive energy analyzer attached to the SEM. The deposit structure and the preferred orientation of crystallites were determined by X-ray diffraction (XRD).

5.2.1. Electrodeposition of Zn-Ni-TiO_2

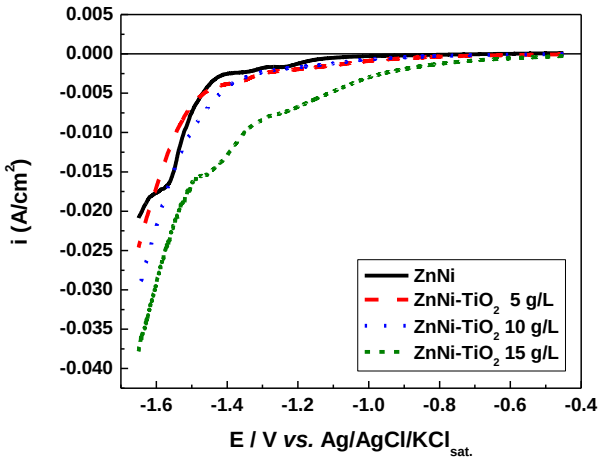

Figure 5.2. Polarization curves obtained during Zn-Ni electrodeposition in the absence and in the presence of TiO_2 nanoparticles.

Figure 5.2 shows polarization curves for codeposition TiO_2 with Zn-Ni alloy, in commercial Performa solution, at variable TiO_2 concentrations.

As seen in Figure 5.2., polarization curves recorded during electrodeposition of Zn-Ni-TiO_2 composite coatings present significant differences depending on the TiO_2 concentration used in the bath. Therefore, at concentrations > 10 g/L TiO_2 particles lead to a positive shift in potential redaction and an increase in the cathodic current [15]. It is possible that at high concentration of nanoparticles (15 g/L), dislocations, chemical heterogeneities or other defects arise in the metal grid and exert a catalytic effect on alloy electrodeposition [16]. Another explanation could consist in stimulating the release reaction of H_2, which is carried out parallel to the alloy deposit.

5.2.2. Electrodeposition of Zn-Ni-Al_2O_3

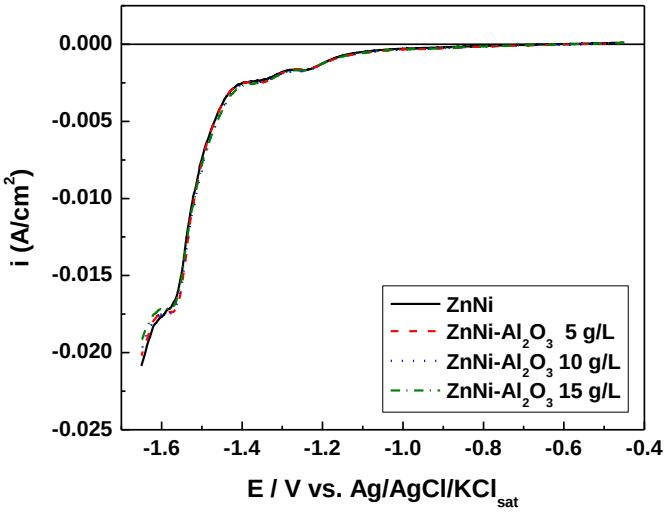

Figure 5.3. Polarization curves obtained during Zn-Ni electrodeposition in the absence and in the presence of Al_2O_3 nanoparticles.

Polarization curves drawn during electrodeposition composite coatings Zn-Ni-Al_2O_3 shown in Figure 5.3, no significant changes are observed between the polarization curves obtained during electrodeposition Zn-NiAl_2O_3 composite coatings at different concentrations of Al_2O_3 nanoparticles used in the plating. Comparing these curves with those obtained when in the bath was added the same concentration of TiO_2 nanoparticles, one can see that the shapes of the curves are different, which shows that the chemical nature of oxidic nanoparticles plays an important role in the electrodeposition process.

5.3.2. XRD analysis

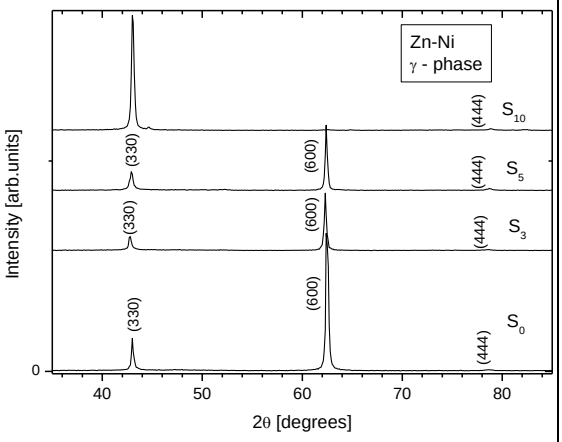

Figure 5.6. XRD of S_0 coating (in the absence of TiO_2 nanoparticles) and samples S_3, S_5 and S_{10} (with 3, 5 and 10 g/L TiO_2, respectively).

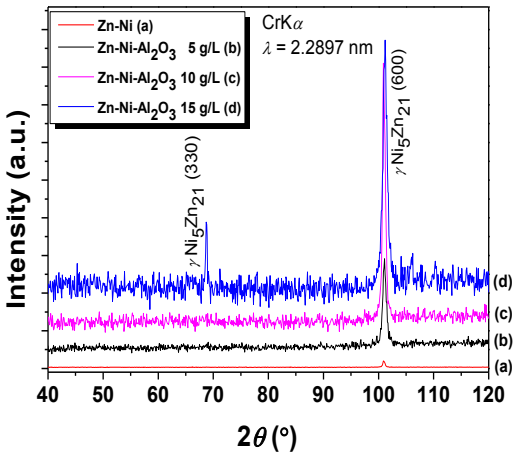

Figure 5.8. X-ray difractograms of Zn-Ni and Zn-Ni-Al_2O_3 coatings obtained with different Al_2O_3 concentrations (5, 10 and 15 g/L).

Figure 5.6. shows XRD pattern for four Zn-Ni coatings samples in the absence and the presence of TiO_2 nanoparticles.

The diffraction peaks for all samples show only the presence of γ-Ni_5Zn_{21} phase.

The absence of TiO_2 peaks suggests that the concentration of phases associated with TiO_2 is under the limit of detection for XRD method, or their dimensions are very small on the nanoscale size [17].

The intensity of (hkl) XRD peaks is proportional to the density of lattice planes. Accordingly, the packing density decreases in the sequence: ρ (110) > ρ (100), [18]. The change of the grain orientations in presence of TiO_2 nanoparticles is indicated by changes of peak intensities. The intensity ratio $r = I_{(330)}/(I_{(330)}+I_{(600)})$ is dependent on TiO_2 content (Table 5.4).

Table 5.4. Data obtained from Zn-Ni and Zn-Ni-TiO_2 coatings, obtained from XRD measurements.

Sample	$\frac{I(330)}{I(330)+I(600)}$ %
S_0 (0 g/L TiO_2)	13
S_3 (3 g/L TiO_2)	23
S_5 (5 g/L TiO_2)	30
S_{10} (10 g/L TiO_2)	99

The change of intensity for the diffraction peaks (330) (or (110)), and (110) (or (600)) shows textural modifications of coatings. The increase of TiO_2 nanoparticles concentration induces an increase of the packing density associated to more closely packed (330) (or (110)) planes.

The results reflecting the grain size of the samples prepared using nanoparticles and blank, are presented in Table 5.5 [17].

Table 5.5. The results of grain size for Zn-Ni samples, in the presence and in the absence of the TiO_2 nanoparticles (concentrație de 3, 5 and 10 g/L).

Sample	B_m [°]	B [°]	2Θ [°]	B [rad]	D [nm]
S_0 blank	0.214	0.151	43.017	0.002634	56.57
S_3 (3 g/L TiO_2)	0.284	0.221	42.770	0.003855	38.62
S_5 (5 g/L TiO_2)	0.348	0.285	42.920	0.004972	29.96
S_{10}(10 g/L TiO_2)	0.259	0.196	43.047	0.003410	43.58

The presence of particles in the metallic deposit may cause change in the crystalline structure of metal layer [19] . Thus, shows that crystal size decreases in the presence of TiO_2 nanoparticles in the bath witness to the blank deposit. The same investigations were performed in the case of Zn-Ni deposits prepared in the presence of Al_2O_3 nanoparticles.

The decrease in crystal size could be explained through the dinamic between the two processes: nucleation and crystal growth in the presence of nanoparticles. The smallest size crystal was obtained at the optimum concentration of TiO_2.

In Figure 5.8, are presented the experimental phases detected in the Zn-Ni and Zn-Ni-Al_2O_3 coatings at difference concentration of nanoparticles in the electrodeposition bath (5, 10 and 15 g/L) [20].

Under the examined conditions, all samples show only the presence of γNi_5Zn_{21} phase, which can lead to a good resistance to corrosion of the deposits. The XRD results are in agreement also with those previously reported for pure Zn-Ni alloys prepared from alkaline electrolytes [3]. At higher Al_2O_3 concentration the γ-phase content increased and a preferred orientation of the crystallites in directions (330) and (600) becomes visible.

For all coatings, the profile of (330) peak exhibits Lorentzian line shape.

Crystallite size calculations were made by using the full width at half maximum of (330) peak, in the Scherer equation:

$$D = \frac{0.9\lambda}{B\cos\theta}$$

and results are presented in Table 5.6.

Table 5.6. Parameters of the Zn-Ni and Zn-Ni-Al_2O_3 coatings, obtained from XRD measurements.

Sample	**Al_2O_3 conc. (g/L)**	**B_m [°]**	**2Θ [°]**	**D [nm]**
Zn-Ni	0	0.453	100.96	40.93
Zn-Ni-Al_2O_3	5	0.702	101.07	26.40
	10	0.558	100.96	33.20
	15	0.899	101.17	20.68

As seen in Table 5.6, the deposit becomes finer grained in the presence of Al_2O_3 due to the fact that the nanoparticles interfere with the nucleation-growth process. Thus, the nanoparticles enhance nucleation by creating disorder in the incorporation of atoms into the lattice or inhibit surface diffusion of atoms towards growing centers and exert a detrimental effect on the crystal growth [19]. This effect of grain refining is beneficial for the corrosion resistance of the deposits.

The change of intensity for the diffraction peaks (330) (or (110)), and 100 (or (600)) shows textural modifications of coatings. The increase of Al_2O_3 nanoparticles concentration in the electrolyte induces an increase of the packing density associated to more closely packed (330) (or (110)) planes in the resulting deposits [20].

5.4. Electrochemical corrosion of composite Zn-Ni-nanoparticles coatings

5.4.2. Open circuit potential

The open circuit potential values for Zn-Ni coatings in the absence and in the presence of TiO_2 nanoparticles are presented in Table 5.7 and in the Table 5.8. are presented for Zn-Ni coatings in the presence and in absence of Al_2O_3 nanoparticles.

Table 5.7. The open circuit potential for Zn-Ni coatings in the absence and in the presence of TiO_2 nanoparticles (conc. 3, 5 and 10 g/L).

Sample	**OCP V *vs.* Ag/AgCl**
ZnNi	- 0.960
ZnNi-TiO_2 3 g/L	- 0.820
ZnNi-TiO_2 5 g/L	- 0.870
ZnNi-TiO_2 10 g/L	- 0.770

In the presence of TiO_2, the OCP is shifted towards more positive values, suggesting an ennoblement of the deposit, equivalent to a breaking of the anodic corrosion process.

Differences between the values obtained for electrodes obtained from solutions containing 5 g/L TiO_2 and 10 g/L TiO_2 is due, probably, to different amount of incorporated TiO_2 or to different roughness of the deposit.

The open circuit potential values for Zn-Ni and Zn-Ni-Al_2O_3 electrodes recorded after 1 h from their immersion in Na_2SO_4 solution (pH 5) are presented in Table 5.8.

Table 5.8. The open circuit potential for Zn-Ni coatings in the absence and in the presence of Al_2O_3nanoparticles (conc. 1, 3, 5, 10 and 15 g/L).

Sample	OCP V *vs.* Ag/AgCl/$KCl_{sat.}$
Zn-Ni	- 0.748
Zn-Ni- Al_2O_3 1 g/L	- 0.720
Zn-Ni- Al_2O_3 3 g/L	- 0.776
Zn-Ni- Al_2O_3 5 g/L	- 0.599
Zn-Ni- Al_2O_3 10 g/L	- 0.788
Zn-Ni- Al_2O_3 15 g/L	- 0.804

As shown in Table 5.8, the corrosion potential of Zn-Ni-Al_2O_3 coatings obtained from solution containing 3, 10 and 15 g/L Al_2O_3, are generally slightly more negative than that of pure alloy, with the exception of 5 g/L Al_2O_3 when a positive shift of the potential is observed, suggesting an ennoblement of the deposit.

These maybe results from the chemical inertia of incorporated aluminium oxide [21], higher percentage than in the previous case.

5.4.3. Polarization curves

5.4.3.1. Zn-Ni-TiO_2 coatings

The results of the polarization tests in 0.2 g/L Na_2SO_4 de pH 5 carried out in a potential range of ± 20mV and ± 200 mV *vs.* OCP using the Zn-Ni coated steel electrodes prepared in presence of different TiO_2 and Al_2O_3 concentrations in the plating bath are presented in Figure 5.9. and Figure 5.10.

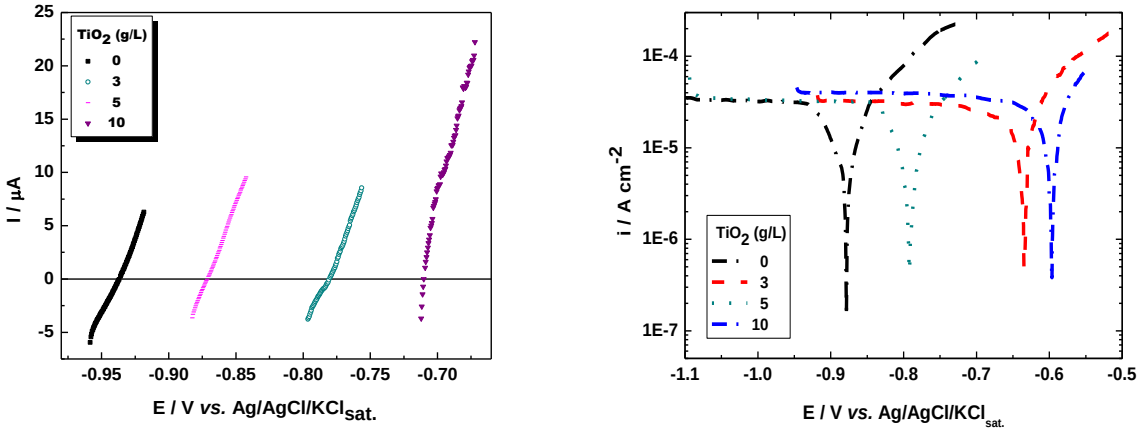

Figura 5.9. Polarization curves drown in 0.2 g/L Na_2SO_4 solution, pH = 5, for the Zn-Ni coated steel (OL37) from alkaline solution containinig TiO_2 nanoparticles in concentration of 3, 5 and 10 g/L; (**A**) ± 20 mV *vs.* OCP domain and (**B**) ± 200 mV *vs.* OCP domain.

The polarization resistance, R_p, was estimated as the inverse of the slope of linear polarization curves, and the corresponding values are presented in Table 5.9. The values of the corrosion parameters for Zn-Ni-TiO_2, are presented in Table 5.9 and Table 5.10 respectively Table 5.11 and Table 5.12 for Zn-Ni-Al_2O_3 coatings [20].

Table 5.9. The R_p values for Zn-Ni coatings in the absence and in the presence of TiO_2 nanoparticles. *Corrosion solution:* 0.2 g/L Na_2SO_4 (pH=5); υ = 0.166 mV/s.

Sample	R_p ($\Omega.cm^2$)	R^2/N
ZnNi	2523	0.998/47
ZnNi-TiO_2 3 g/L	2662	0.998/36
ZnNi-TiO_2 5 g/L	2893	0.999/55
ZnNi-TiO_2 10 g/L	2192	0.998/48

Table 5.10. Kinetic parameters of the corrosion process.

Sample	E_{cor} (V)	i_{cor} (A/cm^2)	b_a (V/dec)	$-b_c$ (V/dec)
ZnNi	- 0.880	$7*10^{-5}$	9.06	1.86
ZnNi-TiO_2 3 g/L	- 0.637	$6*10^{-5}$	6.20	3.82
ZnNi-TiO_2 5 g/L	- 0.792	$2*10^{-5}$	15.18	13.10
ZnNi-TiO_2 10 g/L	- 0.598	$4*10^{-5}$	20.19	3.77

As shown in Table 5.10 an increase in the concentration of TiO_2 nanoparticles, will shift the E_{corr} potential to more positive values. On the other hand a tendency to diminish of corrosion current in the same direction , is observed. The modification of Tafel slope suggests a change in corrosion mechanism in the presence of TiO_2 nanoparticles.

I_{corr} values obtained for Zn-Ni alloy in the presence of TiO_2 nanoparticles are 1.16 times lower for 3 g/L and respectively 1.75 times for 10 g/L TiO_2 nanoparticles than that for Zn-Ni pure value; better results were obtained for the concentration of 5 g/L TiO_2 in the plating bath where the corrosion current decreases to 3.5 times from that of pure Zn-Ni.

5.4.3.2. Zn-Ni-Al_2O_3 coatings

The results of the polarization tests carried out in a potential range of ± 200 mV *vs.* OCP using the Zn-Ni coated steel electrodes prepared in presence of different Al_2O_3 concentrations in the plating bath are presented in the following.

Table 5.11. The R_p values of the Zn-Ni coatings in the absence or in the presence of the Al_2O_3 nanoparticles. *Corrosion solution:* 0.2 g/L Na_2SO_4 (pH=5); υ = 0.166 mV/s.

Sample	R_p ($\Omega.cm^2$)	R^2/N
ZnNi	1534	0.998/11
ZnNi- Al_2O_3 1 g/L	3189	0.973/6
ZnNi- Al_2O_3 3 g/L	3485	0.970/9
ZnNi- Al_2O_3 5 g/L	3652	0.999/13
ZnNi- Al_2O_3 10 g/L	1781	0.999/24
ZnNi- Al_2O_3 15 g/L	2452	0.998/24

As we can see from Table 5.11, in all cases, R_p for all composite coatings is higher than the one for pure Zn-Ni deposit, the highest value was obtained for Zn-Ni-Al_2O_3 deposit with 5 g/L nanoparticles. These results are in accordance with OCP values obtained, suggesting a slow

down of the corrosion desposit and showing the importance of Al_2O_3 nanoparticles concentration in the deposition bath.

Comparing the polarization resistance values, for Zn-Ni deposition in the presence of two types of nanoparticles (TiO_2 şi Al_2O_3), is observed that the highest value of R_p is in the case of 5 g/L Al_2O_3, which should provide the best corrosion resistance, compared with other layers.

To verify this assumption we have examined the polarization curves drawn in a potential range ± 200 mV *vs.* OCP using Zn-Ni coated on steel electrodes prepared in presence of different Al_2O_3 concentrations in the plating bath. The results are presented in Figure 5.10.

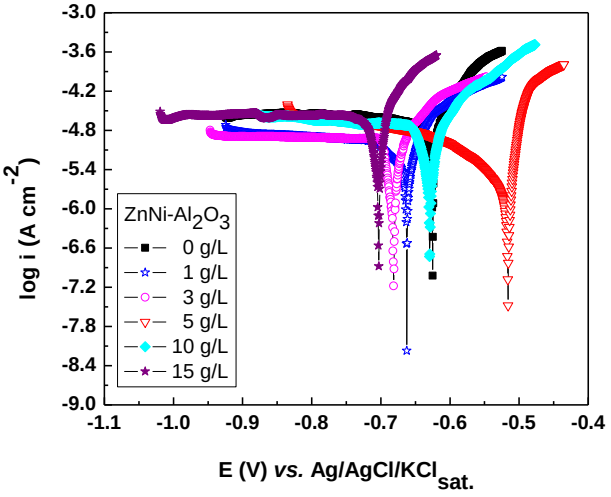

Figure 5.10. Polarization curves obtained from 0.2 g/L Na_2SO_4 solution (pH=5), for OL37 electrodes from alkaline solution containing different concentrations of Al_2O_3 nanoparticles (1, 3, 5, 10 and 15 g/L); in a potential range ± 200 mV *vs.* OCP; scane rate: 0.166 mV/s.

Interpretation by linear regression of the polarization curves in logarithmic form permitted obtaining kinetic parameters of the corrosion process presented in Table 5.12.

As can be seen, the corrosion potential values of the composite layers obtained from solution containing 1, 3, 5 şi 10 g/L Al_2O_3 are more negative than that corresponding to pure Zn-Ni deposit, indicating that the Zn-Ni-Al_2O_3 coatings interact more strongly with the cathodic reaction, in this case the reduction of oxygen. As in the case of OCP values, a relatively important positive potential shift is observed in the case of Zn-Ni-Al_2O_3 coatings prepared with 5 g/L nanoparticles in the plating bath.

Table 5.12. Kinetic parameters of the corrosion process of the Zn-Ni and Zn-Ni-Al_2O_3 conaings on steel.

Sample	E_{corr} (V)	i_{corr} (A/cm^2)	b_a [a] (V/dec)	- b_c [a] (V/dec)	V_{corr} (mm/an) 10^{-2}
Zn-Ni	- 0.616	$2.51*10^{-6}$	0.013	0.014	3.742
Zn-Ni- Al_2O_3 1 g/L	- 0.663	$7.34*10^{-6}$	0.040	0.095	1.095
Zn-Ni- Al_2O_3 3 g/L	- 0.682	$1.65*10^{-6}$	0.013	0.014	2.470
Zn-Ni- Al_2O_3 5 g/L	- 0.516	$1.23*10^{-6}$	0.061	0.014	1.837
Zn-Ni- Al_2O_3 10 g/L	- 0.629	$2.37*10^{-6}$	0.020	0.025	3.546
Zn-Ni- Al_2O_3 15 g/L	- 0.703	$2.57*10^{6}$	0.012	0.017	3.842

[a] b_a and b_c are the anodic and cathodic activation coefficients.

The values of the anodic and cathodic Tafel coefficients calculated for Zn-Ni-Al_2O_3 composite coatings differ from those corresponding to pure Zn-Ni deposit, indicating that the embedded Al_2O_3 nanoparticles influence the kinetics of both anodic and cathodic processes.

The co-deposition mechanism of nanoparticles with the metal involves several steps [22]: (1) formation of ionic clouds on the particles, (2) convection towards the cathode, (3) diffusion through a hydrodynamic boundary layer, (4) diffusion through a concentration boundary layer and finally, (5) adsorption at the cathode where particles are entrapped within the metal deposit. Strongly adsorbed particles are incorporated, while the particles loosely adsorbed on the cathode are swept away from the surface before they are built in. Based on these statements, we supposed that only embedded particles influence the kinetics of electrodeposition and, thus, the Tafel coefficients. It should be mentioned that the decrease of i_{corr} values is more significant also only for Zn-Ni-Al_2O_3 obtained from solutions containing 5 g/L for Zn-Ni- Al_2O_3, proving that, for this concentration, the nanoparticles incorporation in metal deposit has an inhibiting effect on metal corrosion. This effect could be due to a more uniform incorporation of the nanoparticles in the metallic deposit leading to a decrease of the active surface in contact with the corrosive environment. On the other hand, nano alumina particles have a low level of electronic conductivity and when they are uniformly dispersed in the composite coating, they can distract the corrosion current [6].

6. Ti and Ti alloys treated by anodic oxidation in 1 M acetic acid

Anodization of Ti, Ti-6Al-7Nb and NiTi in acetic acid for improving corrosion resistance has been attempted and the corrosion behavior in Hanks solution has been studied in comparison with untreated samples.

6.1. Experimental conditions

Three titanium-based materials are used in the study. Titanium metal (purity 99.6%, annealed) was supplied by Goodfellow (Cambridge, Ltd., UK). Samples of Ti−6Al−7Nb alloy were cut from the femoral component of the total hip replacement manufactured by company Sulzer (Winthertur, Switzerland). Nitinol (NiTi) was a super elastic alloy S, supplied by Memry GmbH, Weil am Rhein, Germany. It was annealed and oxide free with the nominal composition 50 at.% Ni and 50 at.% Ti. Titanium and NiTi were purchased in the shape of a 2 mm-thick foil. Samples were cut from the foil or component in the shape of discs with 15 mm diameter. The samples were mechanically ground under water successively with 320, 500, 800, 1.000, 1.200, 2.400 and 4.000 – grit SiC papers. Each sample was ground in one direction until all imperfections were removed and the surface was covered with a uniform pattern of scratches. The samples were cleaned with ethanol in an ultrasonic bath for two minutes, double-rinsed with Milli-Q water, and finally dried in a stream of nitrogen.

Electrochemical measurements were performed in a conventional three-electrode cell (volume 300 mL) at a temperature of 37 ± 1°C. The working electrode was embedded in a Teflon holder, with an area of 0.785 cm^2 exposed to the solution. The counter-electrode was graphite. Potentials were measured against a saturated calomel electrode (SCE) connected to the cell *via* a Luggin probe. Measurements were carried out with an Autolab PGSTAT 12 potentiostat/galvanostat (Metrohm Autolab, Utrecht, The Netherlands) controlled by Nova 1.7. Corrosion resistance of the deposit was evaluated comparatively by electrochemical measurements, (open circuit potential process took up 2 hours, linear polarization measurements were the performed in the potential range ± 10 mV *vs.* E_{corr}, using a 0.1 mV/s potential scan rate, cyclic polarization in the potential range ± 250 mV *vs.* E_{corr}.

All the electrochemical measurements were performed at 37ºC in simulated physiological solution (SPS) with the following composition: 8 g/L NaCl, 0.4 g/L KCl, 0.25 g/L $NaH_2PO_4 \cdot 2H_2O$, 0.35 g/L $NaHCO_3$, 0.06 g/L $Na_2HPO_4 \cdot 2H_2O$, 0.19 g/L $CaCl_2 \cdot 2H_2O$, 0.4 g/L $MgCl_2 \cdot$

$6H_2O$, 0.06 g/L $MgSO_4 \cdot 7H_2O$, 1 g/L glucose. This solution is known as Hanks balanced salt solution. The pH was adjusted to 7.4 by addition of HCl or NaOH (1M) solution.

Anodic oxidation of the samples was carried out at room temperature in 1 M acetic acid, pH 2.3 for 7200 s at 0.7 V for Ti, Ti-6Al-7Nb and NiTi, and at 3.0 V for Ti and Ti-6Al-7Nb alloy. Acetic acid was supplied by J.T. Baker, The Netherlands.

6.2. Electrochemical characterization

The purpose was to determine the potential for oxidation of Ti and its alloys through plotting the respective polarization curves.

6.2.1. Polarization curves

At first, polarization curves for all three samples of Ti, Ti-6Al-7Nb and NiTi was measured in acetic acid, pH 2.3, to determine the conditions to be used for potentiostatic oxidation.

The polarization curves was measured for Ti, Ti-6Al-7Nb and NiTi in acetic acid 1 M, pH 2.3, after stabilization 5400 s at the open circuit potential are presented in Figure 6.3.

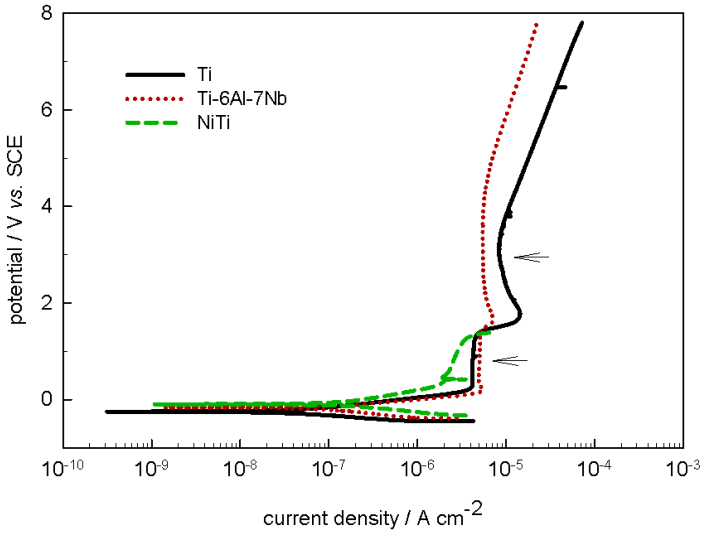

Figure 6.3. Potentiodynamic polarization curves obtained for Ti, Ti-6Al-7Nb and NiTi, in acid acetic 1 M, pH 2.3, using a scane rate: 1 mV/s. The oxidation potentials were: 0.7 V and 3.0 V.

In Tafel region, the current density plateau forms indicating the passivity of all three materials investigated. At approximately 1.0 V the current density starts to increase again. Based on the polarization curves presented in Figure 6.3, the potentials within the well-developed passive state suitable for the

formation of the oxide layer on particular material are selected. For Ti and Ti−6Al−7Nb alloy two potentials are selected: 0.7 V in the first current density plateau, and 3 V in the well-developed second current density plateau. For the NiTi, whose corrosion resistance is much lower than that of other two materials, the potential of 0.7 V is selected. This potential is approximately in the middle of its passive region, and coincides with the first potential selected for the other two materials. The variations of the current density as a function of time recorded during potentiostatic oxidation (anodization) at selected potentials are presented in Figure 6.4.

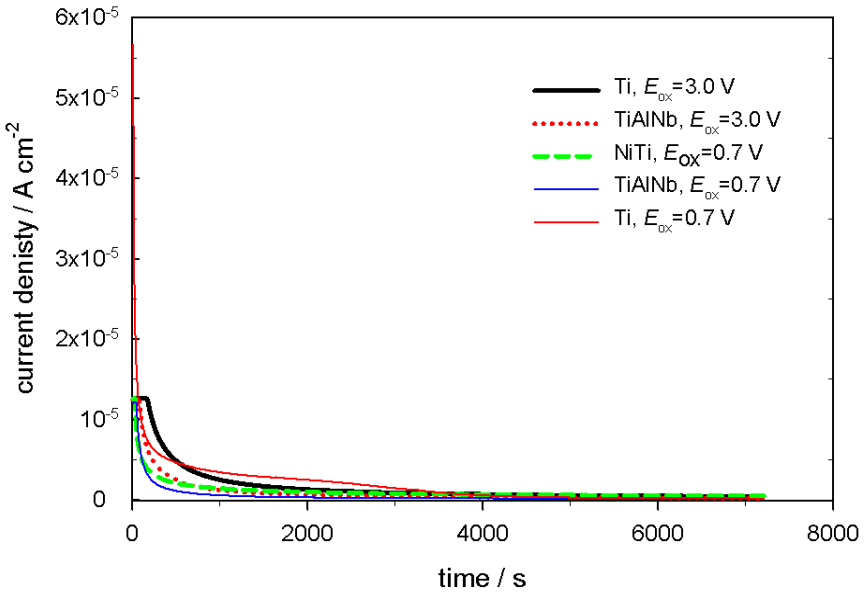

Figura 6.4. Current *vs*. time curves measured during potentiostatic oxidation at 0.7 V and 3.0 V for 7200 s in 1 M acetic acid (pH 2.3).

From Figure 6.4. we observe that, current density values decreases continuously with time until it reaches a steady state after approximately 3000 s and then remains at this low values up to the end of anodization period at 7200 s. This behaviour is related to the growth of passive oxide layer at the surface.

- *Open circuit potential and linear polarization measurements*

The chemical properties of the oxide layer play an important role in biocompatibility of titanium implant and surrounding tissues [23].

Before measurements, samples allowed the registration of OCP. The stabilization process took approximately 2 h and OCP values are presented in Table 6.1.

Table 6.1. The OCP values, measured for Ti, Ti-6Al-7Nb and NiTi in Hank's solution pH 7.4 and 37°C for 5400 s, before and after oxidation in acetic acid (1 M pH 2.3). Oxidation potentials were 0.7 V and 3.0 V.

Sample	**E_{corr} vs. SCE / V**
Untreated	
NiTi	−0.551
Ti	−0.511
Ti−6Al−7Nb	−0.301
After oxidation in acetic acid at 0.7 V	
NiTi	−0.221
Ti	−0.020
Ti−6Al−7Nb	−0.084
After oxidation in acetic acid at 3.0 V	
Ti	−0.209
Ti−6Al−7Nb	−0.098

The value for Nitinol is approximately 250 mV more positive than those for other two materials, this is probably the effect of nickel content in the alloy.

In terms of corrosion nickel is less resistant than titanium and Ti−6Al−7Nb alloy [24].

After anodization in acetic acid, we observe a potential shift towards more positive values indicating that the presence of oxide film protects the base material, while the lossof potential to the negative values indicate dissolution of the film or that it was not formed [25].

The values of linear polarization curves for Ti, Ti-6Al-7Nb and NiTi are presented in Table 6.2, the values of polarization resistance, R_p, were calculated from the slope of *j vs. E* curves measured in a narrow range around E_{corr} (Table 6.4).

Table 6.2. Values of polarization curves measured for Ti, Ti-6Al-7Nb and NiTi before and after oxidation in acetic acid 1 M. *Electrolyte:* Hank's solution (pH 7.4), at +/- 10 mV vs. OCP.

Sample	**R_p (kΩ/cm^2)**
Untreated	
Ti	476
Ti-6Al-7Nb	992
NiTi	253
After oxidation in acetic acid at 0.7 V	
Ti	1719
Ti-6Al-7Nb	1853
NiTi	695
After oxidation in acetic acid at 3.0 V	
Ti	669
Ti-6Al-7Nb	1197

As expected, R_p values, after oxidation are larger than those before oxidation due to the formation of a passive layer on the electrodes surface (Table 6.2). They decrease in the following order: Ti−6Al−7Nb > Ti > NiTi. The highest value of polarization resistance corresponds to the Ti-6Al-7Nb alloy anodized at 0.7 V. When comparing the values before and after oxidation it turns out that the highest relative increase is achieved for titanium oxidized at 0.7 V (3.6 times) and Nitinol (2.7 times).

- *Cyclic polarization measurements*

The testing procedure consisted of monitoring the open circuit potential (OCP) for 5400s and then generating cathodic and anodic polarization curves.

The polarization behavior of the untreated and oxidized samples immersed in Hanks solution is depicted in Figure 6.5.

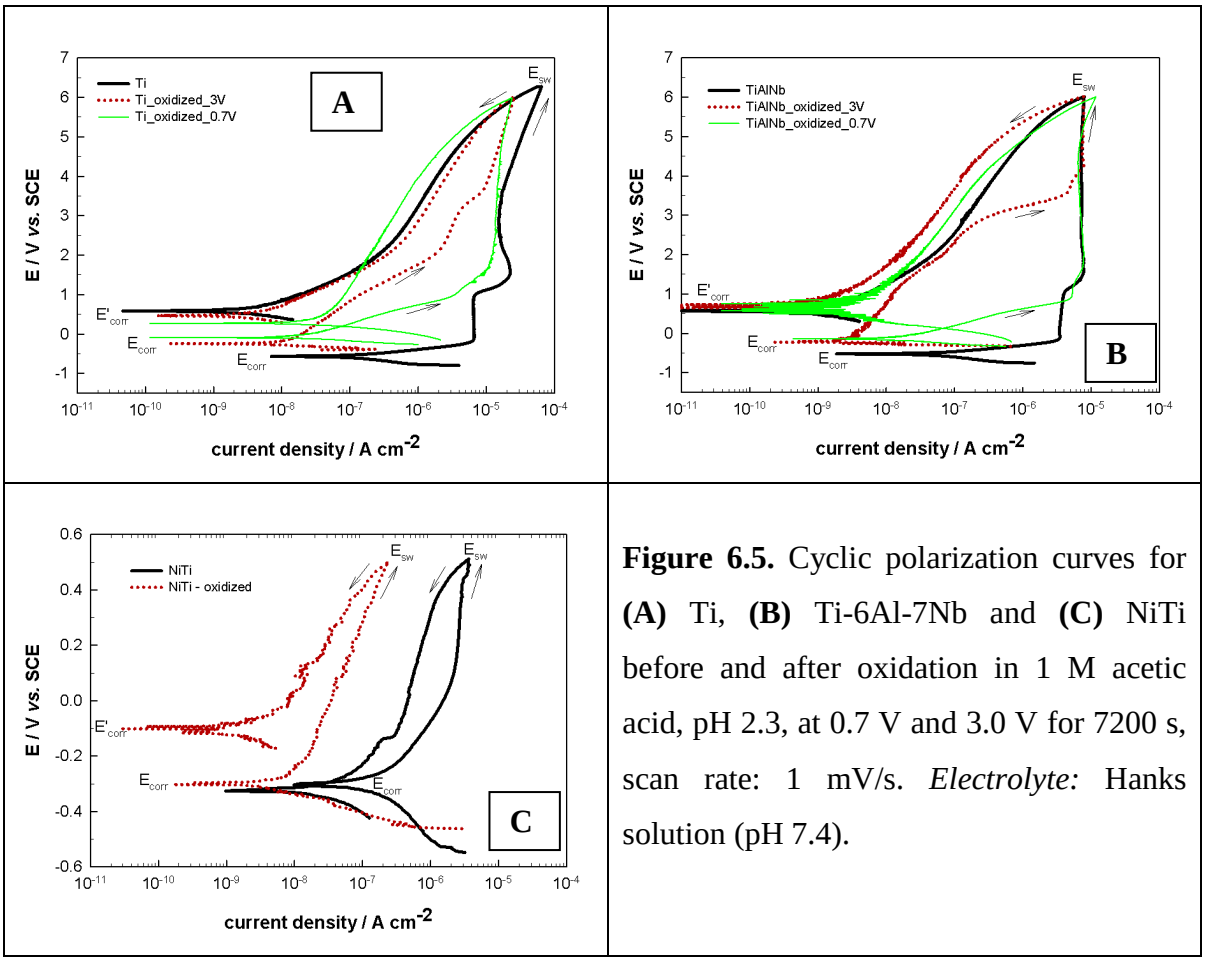

Figure 6.5. Cyclic polarization curves for **(A)** Ti, **(B)** Ti-6Al-7Nb and **(C)** NiTi before and after oxidation in 1 M acetic acid, pH 2.3, at 0.7 V and 3.0 V for 7200 s, scan rate: 1 mV/s. *Electrolyte:* Hanks solution (pH 7.4).

The corrosion parameters (corrosion potential E_{corr}, the corrosion current density i_{corr}) generated from these curves by using Tafel extrapolation and Stern-Geary interpretation are shown in Table 6.3 [26].

Table 6.3. Corrosion parameters measured in simulated physiological solution at pH 7.4, T = 37°C for untreated Ti and after oxidation in 1 M acetic acid for 7200 s at 0.7 V and 3.0 V.

Sample	E_{corr} (V)	i_{corr} (nA/cm^2)	E'_{corr} (V)	ΔE (V)	ΔE' (V)
		Untreated			
Ti	-0.579	97.901	0.693	6.579	5.307
Ti-6Al-7Nb	-0.526	48.364	0.467	6.526	5.533
NiTi	-0.278	422.99	-0.103	0.778	0.603
After oxidation in acetic acid at 0.7 V					
Ti	-0.080	9.590	0.273	6.080	5.727
Ti-6Al-7Nb	-0.139	6.350	0.637	6.139	5.363
NiTi	-0.304	2.474	-0.100	0.804	0.600
After oxidation in acetic acid at 3.0 V					
Ti	-0.274	6.623	0.498	6.274	5.502
Ti-6Al-7Nb	-0.234	1.268	0.717	6.234	5.283

The corrosion behavior of the samples also was characterized by the breakdown potential (E_{bd}), the switching potential (E_{sw}) and the corrosion potential (E_{corr}), extracted from the cyclic polarization curves.

As a measure of the corrosion stability, two parameters were defined (Table 6.3): the difference between the switching potential, $E_{sw,}$ and the corrosion potential in the forward and reverse scan $\Delta E = S_{sw} - E_{corr}$ and $\Delta E' = S_{sw} - E'_{corr,}$ respectively. The broader the value of ΔE and ΔE', the more stable the oxide layer in the forward and reverse scan, respectively.

Following the Tafel region the current density for Ti and Ti−6Al−7Nb increases rapidly up to the first anodic plateau which extends from −0.2 V to 1.0 V, similar for both materials (Figure 6.5 A and B).

The second current density plateau is then formed extending up to the E_{sw}. For Ti metal, a slight increase of current density with potential is observed in the second current plateau, while for the Ti−6Al−7Nb alloy the current density is constant. The highest value of E_{sw} and E_{corr} corresponding to passive behavior of Ti alloy after oxidation at 0.7 V.

The values of Δ*E* are similar for Ti metal (6.579 V) and Ti−6Al−7Nb alloy (6.526 V), and much smaller for NiTi alloy (0.778 V) proving its lower corrosion stability (Figure 6.5 C). After scan reversal, the current density decreases confirming that localized corrosion event was not initiated since otherwise an increase in current density would occur [27]. For Ti and Ti−6Al−7Nb alloy the values of Δ*E*' are for approximately 1 V smaller than the Δ*E* values in the forward scan (Table 6.3). For NiTi, on the other hand, these two values are similar. In other words, the difference (E'_{corr}-E_{corr}) is the largest for

Ti (1.279 V) and the smallest for NiTi (0.078 V). This may be the consequence of variations of rates of oxide film formation and reorganization on various materials.

The formation of oxide layer by anodization in acetic acid strongly affects the polarization behaviour of materials investigated (Figure 6.5). The shapes of the curves are changed and, consequently, also the values of the characteristic corrosion parameters (Table 6.3).

After anodization the E_{corr} values are shifted for approximately 300 mV to 500 mV more positive for Ti and Ti−6Al−7Nb alloy, while for NiTi the shift is only 20 mV. More pronounced differences, up to two orders of magnitude, are observed for the values of j_{corr}. The lowest absolute value of j_{corr} was obtained for the Ti-6Al-7Nb alloy; however, the relative decrease of j_{corr} was the largest for NiTi (170 times) (Table 6.3). These data prove a strong improvement of corrosion resistance in simulated physiological solution induced by the presence of anodized oxide layer.

The potential of anodization in acetic acid affects the shape of the curve subsequently recorded in SPS.

After anodization at 0.7 V, the first current plateau is omitted and the values of current density are up to two orders of magnitude lower compared to untreated sample (Figure 6.5A and B). After oxidation at 3.0 V the current density is further decreased, up to three orders of magnitude. After scan reversal, the curves for untreated and oxidized samples remain similar. The values of ΔE and ΔE' are again close for Ti metal and Ti−6Al−7Nb alloy; the values are slightly lower than for untreated samples due to the shift of E_{corr} to more positive values.

6.3. X-ray photoelectron spectroscopy

The XPS spectra were used to differentiate between various species, *i.e.* to study the chemical environment, whereas spectra obtained, were used for quantifying the chemical composition. XPS was performed with a TFA Physical Electronics Inc. spectrometer using non-abd mono-chromatized Al K_α radiation (1486.6 eV) and a hemispherical analyzer.

- *Composition of the oxide layer*

Based on the XPS survey spectra, the chemical composition of the surface is deduced and presented in Table 6.5.

Table 6.5. Chemical compositions deduced from XPS survey spectra measured at the surface of layers formed by potentiostatic oxidation of Ti, Ti−6Al−7Nb and NiTi in 1 M acetic acid (1 M, pH 2.3) for 7200 s. Oxidation potentials, E_{ox}, were 0.7 V and 3.0 V.

Element	E_{ox} = 0.7 V			E_{ox} = 3.0 V	
	Ti	Ti−6Al−7Nb	NiTi	Ti	Ti−6Al−7Nb
O 1s	42.7	57.2	46.6	55.2	48.8
C 1s	44.7	20.6	38.0	29.5	34.7
Ti 2p	12.6	16.8	13.3	15.3	13.2
Al 2p	-	3.9	-	-	1.8
Nb 3d	-	1.5	-	-	1.5
Ni 2p	-	-	2.1	-	-

The surface contains abundant carbon content due to air contamination during the transfer of the sample from the cell to the XPS chamber. The layer is mainly comprised of titanium and oxygen. The content of Ti and oxygen is the highest on Ti metal, and somewhat lower for the alloys. These results confirm that titanium oxide is the major component of the layer formed by anodization of Ti, Ti-6Al-7Nb and NiTi in acetic acid; however, the oxide layer formed on the alloys contains also minor elements. Besides Ti and O, the layer formed on Ti-6Al-7Nb contains 5.4 and 3.3 at, % aluminum and niobium after oxidation at 0.7 V and 3.0 V, respectively. The layer formed on NiTi contains 2.1 at. % Ni (ratio Ti/Ni is 6.3).

Normalized XPS Ti 2p and O 1s recorded at the surface of Ti, Ti-6Al-7Nb and NiTi oxidized at 0.7 V and 3.0 V are depicted in Figure 6.9.

The centre of the Ti $2p_{3/2}$ peak is located at 459.2 eV confirming the presence of titanium (IV) oxide, TiO_2 (Figure 6.9 a). This is valid for all samples tested. The centre of the O 1s spectra is located at 530.7 eV (Figure 6.9 b).

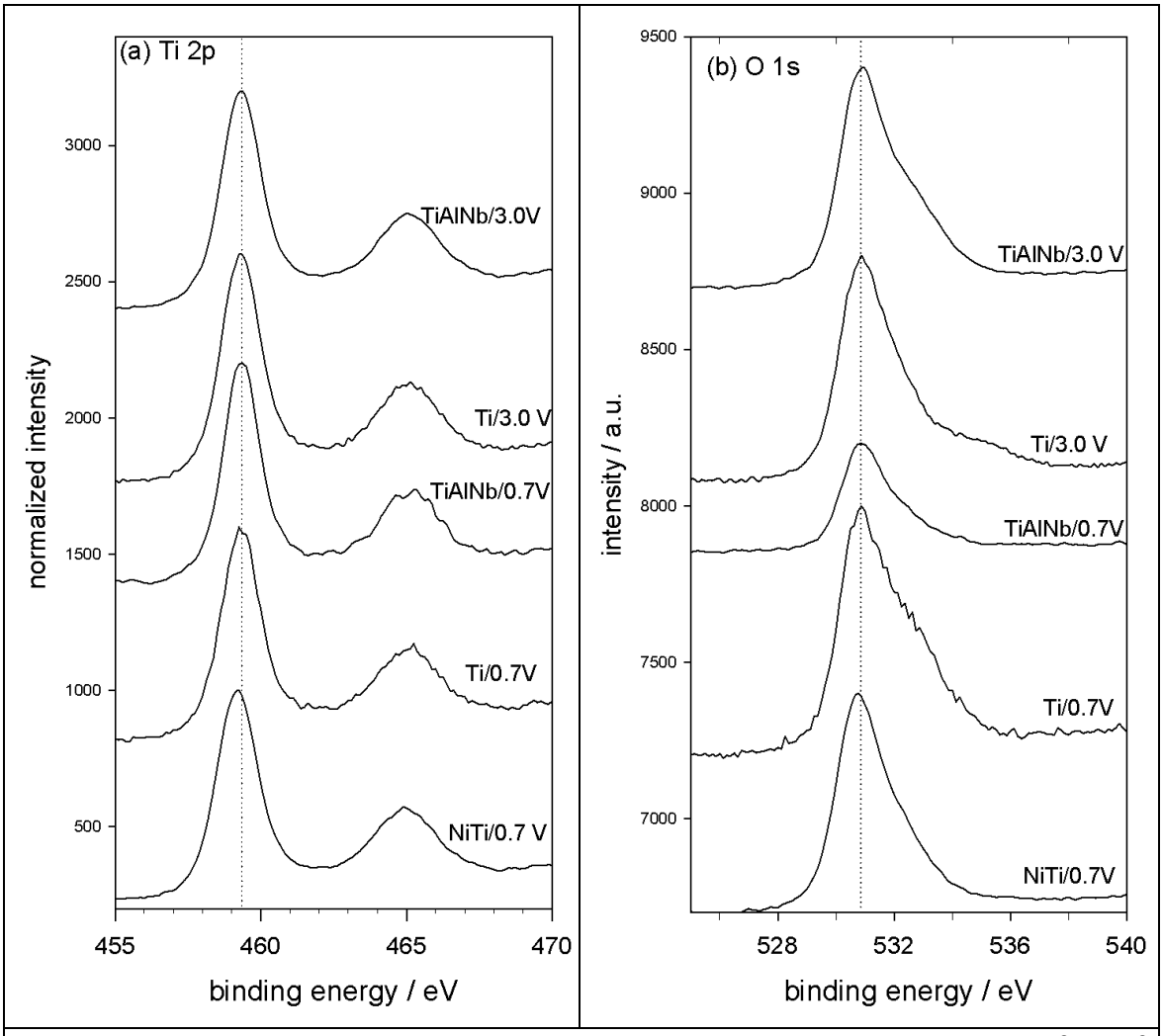

Figure 6.9. Normalized XPS **(a)** Ti 2p and **(b)** O 1s spectra measured at the surface of Ti, Ti-6Al-7Nb and NiTi oxidized at 0.7 V and 3.0 V for 7200 s in 1 M acetic acid.

The intensity of component peaks of Ti, Ti_2O_3 and TiO_2 obtained by deconvolution of the Ti 2p spectra as well the intensities of component peaks O^{2-}, OH^- and H_2O are presented in Table 6.6.

Table 6.6. Intensity of particular component peaks in Ti 2p and O 1s deconvoluted XPS spectra measured at the surface of layers formed by potentiostatic oxidation of Ti, Ti-6Al-7Nb and NiTi in 1 M acetic acid (pH 2.3) for 7200 s. Oxidation potential, E_{ox}, were 0.7V and 3.0V.

Sample / E_{ox}	**Titanium Ti 2p**			**Oxygen O 1s**		
	% Ti	**% Ti_2O_3**	**TiO_2**	**O^{-2}**	**OH^-**	**H_2O**
Ti / 0.7 V	4.6	9.6	85.8	34.5	41.4	24.0
Ti-6Al-7Nb / 0.7 V	3.1	10.0	86.8	27.9	44.8	27.3
NiTi / 0.7 V	4.5	12.5	82.9	43.1	39.5	17.4
Ti / 3.0 V	4.8	9.4	85.8	34.3	40.2	25.5
Ti-6Al-7Nb / 3.0 V	3.3	11.1	85.6	32.5	45.5	24.0

It is evident that, independent of substrate and oxidation potential, the surface layer is mainly composed of TiO_2 (> 80%) and only approximately 10 % of sub-oxide Ti_2O_3. Sub-oxide TiO is not taken into account since its intensity amounted to less than 1 % of total intensity.

Depending on the sample, the oxide component O^{2-} comprised between 27.9 and 43.1 % of the intensity of oxygen spectrum, the rest of intensity belong to hydroxide and water containing oxygen species. Therefore, surface layers formed are strongly hydrated, as expected for air-exposed samples.

- *In-depth composition and thickness of the oxide layer*

In-depth composition and thickness of the layers formed by anodization are revealed by XPS analysis combined with sputtering. Depth profiles are presented in Figures 6.12 and 6.13.

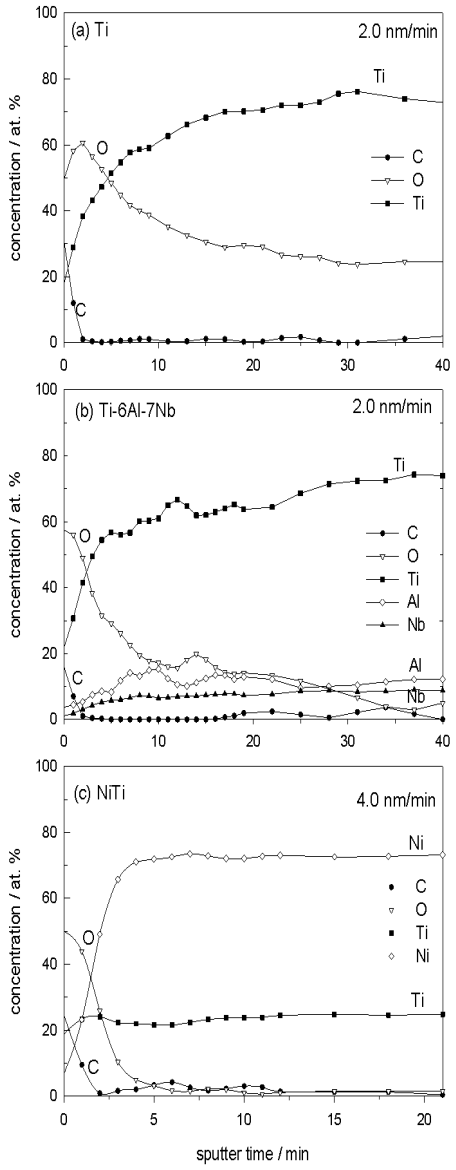

Figure 6.12 Depth profiles of layers formed on **(a)** Ti, **(b)** Ti-6Al-7Nb, and **(c)** NiTi oxidized at 0.7 V. Sputter rate (a and b) 2.0 nm/min, (c) 4.0 nm/min relative to SiO_2 standard.

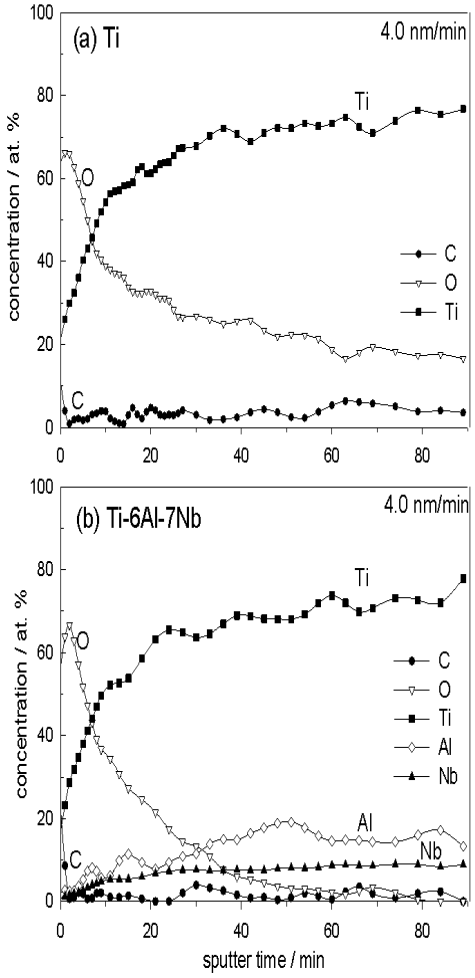

Figure 6.13 Depth profiles of layers formed on **(a)** Ti, **(b)** Ti-6Al-7Nb oxidized at 3.0 V. Sputter rate 4.0 nm/min relative to SiO_2 standard.

The content of carbon decreased as soon after the sputter process begins, in accordance with its presence as surface contaminant. As the sputter process proceeds and the surface oxide is sputtered away, the content of oxygen progressively decreases, and that of titanium increases (Figure 6.12a). For Ti-6Al-7Nb alloy, the contents of Al and Nb increase as well (Figure 6.12b) and for NiTi alloy, the sputtering process induces a strong enrichment of Ni due to preferential sputtering of this element (Figure 6.12b) and for NiTi alloy, the sputtering process induces a strong enrichment of Ni due to preferential sputtering of this element (Figure 6.12c) [28]. Similar behavior of Ti and Ti-6Al-7Nb alloy was observed also after oxidation at 3.0 V (Figure 6.13.)

7. GENERAL CONCLUSIONS

1. Zn-Ni electrodeposition from the alkaline home-made plating bath:

- the presence of additives allowed the obtaining of more compact and brighter Zn-Ni deposits than in their absence and, in case of some combinations of additives (PEG+ Vanillin), a decrease of corrosion current density of the electrodeposited coatings was noticed; with an order of magnitude;

- the presence of TiO_2 nanoparticles in the plating bath does not lead to a significant decrease of corrosion current density of the resulting coatings, even in the presence of the optimal combination of additives.

2. Zn-Ni electrodeposition from the commercial alkaline electrolyte:

- the coatings obtained by use of commercial electrolyte led to compact, leveled and bright Zn-Ni deposits;

- the incorporation of-nanoparticles in Zn-Ni coatings by electrodeposition influenced the corrosion behavior of the composite deposits, exerting either a beneficial, or a harmful effect, depending on the nanoparticles nature and concentration;

- Al_2O_3 nanoparticles confer to Zn-Ni deposits a greater corrosion protection than TiO_2 nanoparticles, influencing the corrosion process, in terms to its bracking;

- the concentration of nanoparticles in the plating bath affects the corrosion resistance of the resulting composite layers. Under the examined conditions, the existence of an optimal concentration was pointed out, which was proven to be 5 g/L both in the case of Al_2O_3 and of TiO_2.

The existence of an optimal concentration of nanoparticles in the plating bath is the result of existence of two contrary effects which are the consequence of their incorporation in the metallic matrix: a beneficial one (the embedded inert oxide particles diminish the active surface in contact with the corrosive environment) and a detrimental one (in higher concentration they disturb the electrocrystallization process creating defects which may enhance corrosion).

3. Preparation of oxide layers on Ti and Ti-alloys

- Anodization of Ti, TiAlNb and NiTi in acetic acid and the formation of TiO_2 on the substrate, beneficially affect the corrosion behavior of all three materials in simulated physiological solution. This is evidenced by a shift of the corrosion potentials to more positive values, an increase in the polarization resistance and a decrease in corrosion current densities.

- The main oxide component formed by anodization on Ti, Ti-6Al-7Nb and NiTi in acetic acid was titanium oxide, TiO_2.

- The composition of oxide layer is similar on all three substrates; the thickness of the oxide layer differs depending on the oxidation potential and type of substrate.

- After anodization Ti, Ti-6Al-7Nb and NiTi, the Ti-6Al-7Nb alloy expresses the best protective corrosion behavior in simulated physiological solution.

- The polarization resistance values corresponding to the oxidized Ti−6Al−7Nb alloy during the later stages of immersion are one order of magnitude higher than those determined for the same untreated alloy, confirming that the anodised samples possess a much higher corrosion resistance than the untreated ones.

- The significant enhancement of the polarisation resistance values at the higher immersion time of anodically oxidized Ti-6Al-7Nb alloy in Hank's physiological solution could be due to the stabilization of the barrier layer, which might diminish the corrosion tendency of the alloy.

8. SELECTED REFERENCES

1. F.J. Fabri Miranda, O.E. Barcia, S.L. Diaz, O.R. Mattos, R. Wiart, *Electrodeposition of Zn-Ni alloys in sulfate electrolytes.* Electrochimica Acta, 1996. **41**: p. 1041-1049.
2. V.G. Roev, R.A. Kaidrikov, A.B. Khakimullin, *Zinc-Nickel Electroplating from Alkaline Eletrolytes Containing Amino Compounds.* Russian Journal of Electrochemistry, 2001. **37**: p. 756-759.
3. L.S. Tsybulskaya, T.V. Gaevskaya, O.G. Purvskaya, T.V. Byk, *Electrochemical deposition of zinc-nickel alloy coatings in a polyligand alkaline bath.* Surface and Coatings Technology, 2008. **203**: p. 234-239.
4. M.M. Abou-Krisha, H.M. Rageh, E.A. Matter, *Electrochemical studies on the electrodeposited Zn-Ni-Co ternary alloy in different media.* Surface & Coatings Technology, 2008. **202**: p. 3739-3746.
5. M.M. Abou-Krisha, F.H. Assaf, S.A. El-Naby, *Electrodeposition behavior of zinc-nickel-iron alloys from sulfate bath.* Journal of Coatings Technology and Research, 2009. **6**: p. 391-399.
6. H. Zheng, M. An, J. LU, *Corrosion behavior of Zn-Ni-Al_2O_3 composite coatings.* Rare Metals, 2006. **25**: p. 174-178.
7. M.E. Soares, C.A.C. Souza, S.E. Kuri, *Corrosion resistance of a Zn-Ni electrodeposited alloy obtained with a controlled electrolyte flow and gelatin additive.* Surface & Coatings Technology, 2006. **201**: p. 2953-2959.
8. ASM Handbook, *Alloys Phase Diagrams.* The Materials Information Company, 1992. **3**: p. 1247-1249.
9. H.Y. Lee, S.G. Kim, *Characteristics of Ni deposition in an alkaline bath for Zn-Ni alloy deposition on steel.* Surface & Coatings Technology, 2000. **135**: p. 69-74.
10. I. Milošev, T. Kosec, H.-H. Strehblow, *XPS and EIS study of the passive film formed on orthopedic Ti-6Al-7Nb alloy in Hank's physiological solution.* Electrochimica Acta, 2008. **53**: p. 3547-3558.
11. L.M. Muresan, J. Eymard, D. Blejan, E. Indrea, *Zn-Ni alloy coatings from alkaline bath containing, triethanolamine. Influence of additives.* Studia Universitatis Babeș-Bolyai, Chemia, 2010. **LV (1)**: p. 37-44.

12. M.Stern, A.L. Geary, *Electrochemical Polarization: I. A theoretical analysis of the shape of polarization curves.* Journal of The Electrochemical Society, 1975. **104**: p. 56-63.
13. D. Blejan, D. Marconi, A. Pop, L.M. Muresan, *The influence of TiO_2 nanoparticles on morpho-structural and anti-corrosion properties of electrodeposited Zn-Ni coatings.* Studia Universitatis Babeş-Bolyai, Chemia, 2011. **LVI (1)**: p. 95-105.
14. M.S. Chandrasekar, S. Srinivasan, M. Pushpavanam, *Properies of Zinc alloy electrodeposits produced from acid and alkaline electrolytes.* Journal of Solid State Electrochemistry, 2009. **13**: p. 781-789.
15. G. Wu, N. Li, D.L. Wang, D.R. Zhou, B.Q. Xu, K. Mitsuo, *Effect of α-Al_2O_3 paricles on the electrochemical codeposition of Co-Ni alloys from sulfamate electrolytes.* Materials Chemistry and Physics 2004. **87**: p. 411-419.
16. A. Lozano-Morales, E.J. Podlaha, *The effect of Al_2O_3 nanopowder on Cu electrodeposition.* Journal of The Electrochemical Society, 2004. **151**: p. C478-C483.
17. D. Blejan, D. Bogdan, M. Pop, A.V. Pop, L.M. Muresan, *Structure, morphology and corrosion resistance of Zn-Ni-TiO_2.* Optoelectronics and Advanced Materials – Rapid Communications, 2011. **5**: p. 25-29.
18. F. Mansfeld, S. Gilman, *The Effect of Lead Ions on the Dissolution and Deposition Characteristics of a Zinc Single Crystal in 6N KOH.* Journal of The Electrochemical Society, 1970. **117**: p. 588-592.
19. C.T.J. Low, R.G.A. Wills, F.C. Walsh, *Electrodeposition of composite coatings containing nanoparticles in a metal deposit.* Surface and Coatings Technology, 2006. **201**: p. 371-383.
20. D. Blejan, L.M. Muresan, *Corrosion behavior of Zn-Ni-Al_2O_2 nanocomposite coatings obtained by electrodeposition from alkaline electrolytes.* Materials and Corrosion, 2012. **DOI: 10.1002/maco.201206522**
21. H.Y. Zheng, M.Z. An, *Electrodeposition of Zn-Ni-Al_2O_3 nanocomposite coatings under ultrasound conditions.* Journal of Alloys and Compounds, 2008. **459**: p. 548-552.
22. J.R. Roos, J.P. Celis, J. Fransaer, C. Buelens, *The Development of Composite Plating for Advanced Materials.* Journal of the Minerals & Materials Society, 1990. **42**: p. 60-63.

23. N.A. Al-Mobarak, A.A.A.-S., F.A. Al-Rashoud, *Corrosion behavior of Ti-6Al-7Nb alloy in biological solution for denstistry applications.* International Journal of Electrochemical Science, 2011. **6**: p. 2031-2042.
24. I. Milošev, B. Kapun, *The corrosion resistance of Nitinol alloy in simulated physiological solutions Part 1: The effect of surface preparation* Materials Science and Engineering C, 2012. **32**: p. 1087-1096.
25. I. Gurappa, *Characterization of different materials for corrosion resistance under simulated body fluid conditions.* Materials Characterization, 2002. **49**: p. 73-79.
26. I. Milošev, D. Blejan, S. Varvara, L. M. Muresan, *Effect of anodic oxidation on the corrosion behaviour of Ti-based materials in simulated physiological solution.* Materials Chemistry and Physics, trimis spre publicare.
27. Z. Szklarska-Smialowska, *Pitting Corrosion of Materials.* National Association of Corrosion Engineers, 1986. **Houston, Texas**.
28. I. Milošev, B. Kapun, *The corrosion resistance of Nitinol alloy in simulated physiological solution Part 2: The effect of surface treatment.* Materials Science and Engineering C, 2012. **32**: p. 1068-1077.

9. List of publications

A. Articles

I. L.M. Muresan, J. Eymard, **D. Blejan**, E. Indrea, *Zn-Ni alloy coatings from alkaline bath containing, triethanolamine. Influence of additives*, Studia Universitatis Babeş-Bolyai, Chemia, LV (1) (**2010**) 37-44.

II. **D. Blejan**, D. Bogdan, M. Pop, A.V. Pop, L.M. Muresan, *Structure, morphology and corrosion resistance of Zn-Ni-TiO_2 composite coatings*, Optoelectronics and Advanced Materials – Rapid Comunications, 5 (1) (**2011**) 25-29.

III. **D. Blejan**, D. Marconi, A. Pop, L.M. Muresan, *The influence of TiO_2 nanoparticles on morpho-structural and anti-corrosion properties of electrodeposited Zn-Ni coatings*, Studia Universitatis Babeş-Bolyai, Chemia, LVI (1) (**2011**) 95-105.

IV. **D. Blejan**, L.M. Muresan, *Corrosion behavior of Zn-Ni-Al_2O_2 nanocomposite coatings obtained by electrodeposition from alkaline electrolytes*, Materials and Corrosion, **DOI**: 10.1002/maco.201206522 (**2012**).

V. I. Milošev, **D. Blejan**, S. Varvara, L. M. Muresan, *Effect of anodic oxidation on the corrosion behaviour of Ti-based materials in simulated physiological solution*, Materials Chemistry and Physics, trimis spre publicare.

B. Comunications

1. **D. Blejan**, J. Eymard, E. Indrea, L.M. Muresan, **2010**, "Influence of additives on Zn-Ni alloy deposition from alkaline bath containing triethanolamine, *Special edition, Molecular Modeling in Chemistry and Biochemistry*, Cluj-Napoca, ROMANIA, 28 May (**poster**).

2. **D. Blejan,** J. Eymard, E. Indrea, L.M. Muresan, **2010**, „Zn-Ni alloy coatings from from alkaline bath containing triethanolamine: Influence of additives", *Second Regional Symposium on Electrochemistry South-East Europe*, Belgrade, SERBIA, 6-10 June (**poster**).

3. **D. Blejan**, D. Marconi, A. Pop, L.M. Muresan, **2010**, "Corrosion investigation of composite Zn-Ni-TiO_2 coatings obtained by electrolytic codeposition"**,** *The 5th National Conference with International Participation, Corrosion and Anticorrosive Protection,* Cluj-Napoca, ROMANIA, 16-18 September (**oral communication**).
4. **D. Blejan**, L.M. Muresan, **2011**, "Composite coatings with improved corrosion resistance obtained by co-electrodeposition of Zn-Ni with Al_2O_3 nanoparticles", *International U.A.B. – B.E.N.A. Conference Environmental Engineering and Sustainable Development,* Alba-Iulia, ROMANIA, 26-27 May, (**poster**).
5. **D. Blejan**, I. Milošev, L.M. Muresan, **2011**, "The corrosion resistance of titanium and its alloys in simulated physiological solution", *The 6th National Conference with International Participation, Corrosion and Anticorrosive Protection,* Cluj-Napoca, ROMANIA, 22-24 Semptember (**oral communication**).
6. **D. Blejan**, L.M. Muresan, **2012**, „ZnNi-TiO_2 and ZnNi-Al_2O_3 composite coatings obtained by electrolytic codeposition", *Third Regional Symposium on Electrochemistry South-East Europe,* Bucuresti, ROMANIA, 13-17 May (**poster**).
7. **D. Blejan**, G. Žerjav, L.M. Muresan, I. Milošev, **2012**, „Improvement in corrosion resistance of Ti and Ti-6Al-7Nb by anodization in acetic acid", *Third Regional Symposium on Electrochemistry South-East Europe,* Bucuresti, ROMANIA, 13-17 May (**poster**).